

Article

# Synthesis of SiO<sub>2</sub> Coated Ag-Cicada Wing as Large Scale Surface Enhanced Fluorescence Substrate

Siye Pan <sup>1</sup>, Yanying Zhu <sup>1,\*</sup>, Guochao Shi <sup>1</sup>, Zubin Shang <sup>1</sup>, and Mingli Wang <sup>1,\*</sup>

<sup>1</sup> State Key Laboratory of Metastable Materials Science & Technology and Key Laboratory for Microstructural Material Physics of Hebei Province, School of Science, Yanshan University, Qinhuangdao, Hebei 066004, P.R. China

\* Correspondence: yyzhu@ysu.edu.cn (Y.Z.); wml@ysu.edu.cn (M.W.)

**Abstract:** The surface enhanced fluorescence (SEF) detection bases by plasmonic nanopillars array with nanoparticles has opened up a new gate in the application of biological imaging and sensing. The fluorescence enhancement of the probe molecule depends on its position in equilibrium, which is close to the hot spot leading to the electromagnetic field enhancement, but not too close to the metal surface resulting in quenching. Here, a large scale SiO<sub>2</sub>-Ag-cicada wing SEF substrate was fabricated by magnetron sputtering with correction enhancement factor of 797.6. Thereinto the cicada wing provides the skeleton of the nanopillars array structure, the deposited Ag constructs two kinds of hot spots, and SiO<sub>2</sub> forms a separation layer to prevent quenching. Moreover, the substrate exhibited good reproducibility, high sensitivity with low limits of detection (LOD) and high stability for oxidation resistance. We propose that SEF substrate with modification of SiO<sub>2</sub> can not only improve the enhancement performance, but also expanding its application in the biological investigations.

**Keywords:** surface-enhanced fluorescence; quenching; Rhodamine 6G; hot spot; separation layer; high reproducibility;finite difference time domain

## 1. Introduction

Fluorescence-based techniques such as biosensing [1], bioimaging [2], low volume detection [3], and specific immunodiagnosis [4] are heavily dependent on emerging surface-enhanced fluorescence (SEF) technology to detect target fluorescent. High performance in reproducibility, sensitivity and stability is in urgent need for SEF applications. There are two mechanisms involved in the SEF process, which are the enhanced emission and the quenching [5-7]. The former is proportional to the square of the electromagnetic(EM) enhancement and increases when the distance between surface and emitter decreases [8]. The latter dues to energy transfer to nonradiative surface plasmons [9,10]. The quantum yield, the ratio between the EM enhanced radiative decay rate and the total decay rates, also decreases when the distance between emitter and surface decreases [11]. A delicate balance between these two factors indicated an optimal surface-emitter distance to obtain maximum enhancement.

Due to remarkable LSPR properties in the visible region ,the substrate of noble metal nanoparticles with a certain size on the surface was proved to greatly improve the performance of SERS and SEF [12]. H. Szmecinski et al have studied the enhanced fluorescence of three spectrally distinct fluorophores on periodic arrays of silver nanoparticles with different size, shape, spacing, and height of on the fluorescence enhancement [13]. Arrays of sub-wavelength holes (nanoholes) in gold films were used as a substrate for SEF in A.G.Brolo et al's study [14]. A maximum enhancement of close to 2 orders of magnitude as compared to the emission of films on glass was obtained. From above studies, period array structure not only has large electromagnetic enhancement, but also is

easy to study the size and morphology systematically. Cicada wing has a long-range period nanopillars array structure, is the ideal material for fabricating SEF substrate.

Many groups studied into the distance dependant enhanced fluorescence theoretically and experimentally. Chris D. Geddes et al. attached the fluorophores with 19b labeled DNA (dye-metal distance  $D \approx 10$  nm) to silver islands films (SIFs), resulting fluorescence signals were enhanced eightfold than labeled DNA in free state, (MEF is about  $\approx 80$ ). And in shorter distance ( $D \approx 2$  nm), MEF reached 360 [15]. By controlling the length of DNA, it can control the distance and act as the separation layer. According to K. Ray et al.'s work a maximum of a 6-fold increase in the fluorescence intensity from a monolayer of the sulforhodamine B at a distance of 9 nm from the metal-nanostructured surface, with the enhancement decreasing down to 1.5-fold at about a 30 nm separation distance [16]. From above studies, it seems that the optimal distance of fluorescence enhancement varies, which was determined by respective morphology, shape and size of metal nanostructures. However, the maximum enhancement can not be obtained by simply shortening the distance. There are three problems that have hindered the practical applications of the bare metal in SEF. Firstly, the nanoparticles and target molecules will form direct bonding, which will change the electronic and geometrical structures [17]. As a consequence the Raman and fluorescence spectra of the molecule will change accordingly, the substrate will be no longer suitable for detection. Secondly, Even without direct bonding, the close contact between the molecule and the metal NPs could lead to strong fluorescence quenching which is harmful to SEF [18]. Thirdly, the bare metal could be easily oxidized under chemical environments which will lead to significant decreases to the EM enhancement and, thus, the Raman and fluorescence signals. It's necessary to coat a shell of inactive materials on the metallic surface for conquering the weakness mentioned above.  $\text{SiO}_2$  was chosen as coating materials for its chemically inert, antioxidant and non-toxic property [19,20].  $\text{SiO}_2$  is widely used as an separation layer in single-molecule fluorescence detection, but rarely used in synthesis of large-scale substrates for enhancing spectrum measurement [21].

In current work, Ag-cicada wing and  $\text{SiO}_2$  coated Ag-cicada wing SEF substrates with various thickness were fabricated by magnetron sputtering, as illustrated in Figure 1. In the previous work, SERS substrate was prepared with a similar method to achieve detection [22,23]. The structure was composed of nano-particles, and nano-pillars array. Rhodamine 6G (R6G) was selected as reporter molecule and the intensity of fluorescence signals were enhanced because of the effect of surface plasmon resonance and two types of "hot spots". The distribution of electric field is simulated by 3d finite-difference time-domain method and the location of hot spot is analyzed. The Ag-cicada wing substrate with separation layer or not got excellent reproducibility. Moreover, the substrate exhibited sensitivity with the limits of detection (LOD) as low as  $1 \times 10^{-7}$  mol/L. Excellent antioxidant capacity was obtained after  $\text{SiO}_2$  was introduced as space layer. We consider that SEF substrate with high reproducibility and stability has broad application prospects in biomedical investigations.

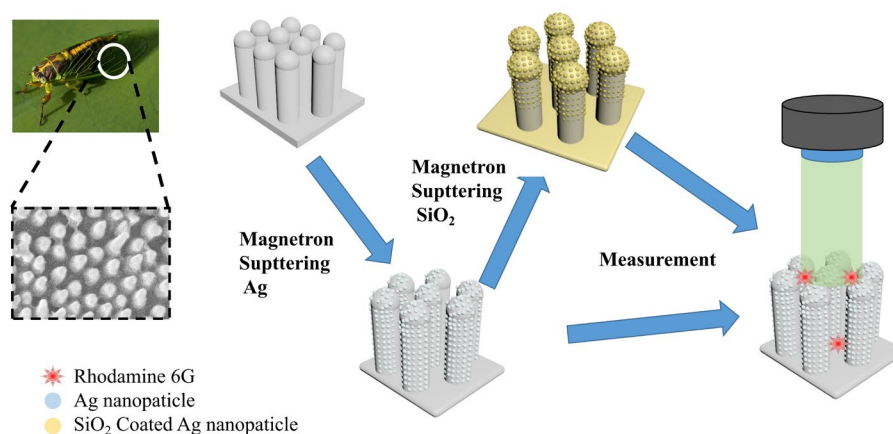


**Figure 1.** Schematic diagram of the fabrication process of the Ag-X substrates and SEF measurement by fluorescent system.

## 2. Materials and Methods

### 2.1. Sample preparation

Prior to preparing the samples, the cicada wings were washed with absolute ethanol for 5 minutes and then rinsed with deionized water for 5 minutes to remove contaminants. The transparent region was then cut into a 1 cm x 1 cm square block as a SEF substrate template. Ag nanofilms were sputtered on the cicada wings using a radio frequency magnetron sputtering system (DHRM-3). The sputtering target of silver (99.99%) and SiO<sub>2</sub> (99.99%) were purchased from ZhongNuo Advanced Material (Beijing, China) Technology Co., Ltd. C.W.s were purchased from Beijing Jiaying Grand Life Sciences Co., Ltd. Experiments with cicada wing complied with the accepted ethical standards and were approved by the Ethical Review Board of Yanshan University on 15 January 2018. The sputtering time has a good control of the height of the Ag nanoparticle layer. In order to find the best SEF enhancement performance, the sputtering time was set to 20, 22.5, 25, 30 and 40 minutes, and the corresponding substrate names were Ag-C.W.-20, Ag-C.W.-22.5, Ag-C.W.-25, Ag-C.W.-30, Ag-C.W.-40, the chamber pressure before and in sputtering was set to  $3.0 \times 10^{-3}$  pa and 1.1 pa, respectively. The sputtering voltage was 140V, and the current was 110 mA.

The shell could effectively protect the NPs from oxidation and avoids the direct contact between the metallic layer and the reporter. SiO<sub>2</sub> was further sputtered on the substrate of Ag cicada wings with different sputtering time. The sputtering voltage was 140 V, and the current was 120 mA. the chamber pressure before and in sputtering was change to  $3.0 \times 10^{-3}$  pa and 5 pa, respectively. The sputtering time was set to 10, 16, 27 seconds.

### 2.2. Surface Characterization

The surface morphology of the winged and Ag-cicada wing was characterized by field emission scanning electron microscopy (FE-SEM, Model 7593-H). The chemical composition and the phase of substrates were analyzed by X-ray diffraction (D/MAX-2500/PC).

### 2.3. Absorption Spectroscopy

Cicada wing, Ag-C.W.-20 substrate, Ag-C.W.-22.5 substrate and aqueous  $10^{-5}$  M R6G were measured with ultraviolet to visible absorption spectrometer (Hitachi U-3900) in the wavelength range from 200 to 700 nm.

### 2.3. Fluorescence Spectroscopy

R6G were purchased from J&K scientific LTD. And their solutions with various concentrations were diluted in Deionized water with 18 MΩ·cm resistivity.

The effect of sputtering time on fluorescence intensity was analyzed by a fluorescence spectrophotometer (Hitachi F-7000). The fluorescence spectrophotometer was set to an excitation wavelength of 500 nm for R6G. For steady-state measurements, the scan speed was set to be 1200 nm/min. The excitation and emission slit width of the fluorescence spectrophotometer were set to be 5 nm.

A lot of the applications of fluorescence are biological and medical, and vivo testing almost in the liquid environment, this measurement is to get fluorescence data in the liquid phase environment. The two glass sheets and the sample between them formed a sandwich structure. The sample was then placed in a fluorescence spectrometer for measurement.

## 3. Results and Discussion

### 3.1. Topography of Nanostructure on Bio-metallic Substrate

The FE-SEM image of the nanostructure is shown in Figure 2. As can be seen from the top view of FE-SEM Figure 2.(b), the ordered arrangement of the mastoid structures is a unique feature of the cicada wings. Magnetron sputtering causes Ag nanoparticles to form a nanoisland on top of the

mastoid. As the sputtering time increases, the mastoid structure becomes a cylinder with a nanosphere cap as a whole, and the diameter of the top ball cap increases. The gap between the columns gradually becomes smaller. Figure 2.(a), the untreated cicada wing substrate side view shows its layer height, 200 nm on average. The average size of the top sphere were measured, where a total of 100 nano-particles were measured to obtain an average dimension on every kind of substrates, and shown in the table below. Table 1. revealed that under a certain deposition velocity, the size of the formed spherical top does not increase linearly, which is mainly caused by the structure of cicada wings itself. Figure 2.(g) and (h) show the morphology of SiO<sub>2</sub> sputtering at 16s and 27s on Ag-C.W.-30 substrate. Too much SiO<sub>2</sub> filled the gaps as illustrated in Figure 2.(h).

**Table 1.** The relationship between sputtering time, average size of top sphere, average gap width.

Sputtering time (min)	Diameter of spherical top (nm)	Gap width (nm)
20	144.57	40
22.5	164.81	34
25	185.39	14
30	192.89	7

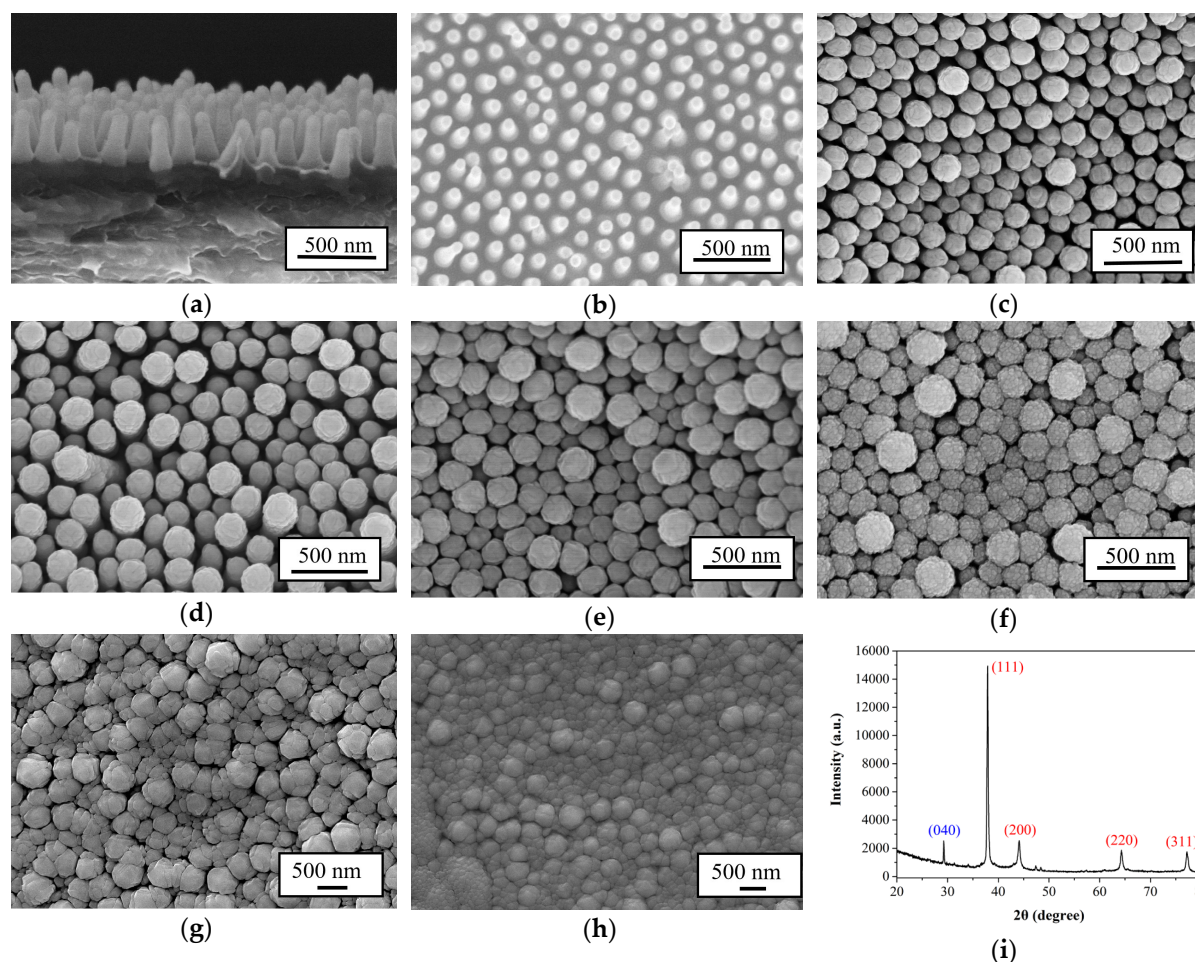


**Figure 2.** Typical FE-SEM images of cicada wing surface. (a)side view of cicada wing; (b)top view of cicada wing; FE-SEM images of Ag-C.W.-x substrates obtained with different sputtering time. (c)Ag-C.W.-20 substrate; (d)Ag-C.W.-22.5 substrate; (e)Ag-C.W.-25 substrate; (f)Ag-C.W.-30 substrate; (g)Ag-C.W.-30 substrate after SiO<sub>2</sub> sputtering for 16s; (h)Ag-C.W.-30 substrate after SiO<sub>2</sub> sputtering for 27s; (i) XRD pattern of SiO<sub>2</sub>-Ag-C.W. substrate.

Figure 2.(i) illustrates the XRD pattern of SiO<sub>2</sub>-Ag-C.W. substrates, and it is clear that when the values of 2 $\theta$  are 38.1, 44.4, 64.3 and 77.3, they correspond to (111), (200), (220) and (311)

crystallographic planes of face-centered cubic Ag phase (JCPDS 04-0783), respectively. And the values of  $2\theta$  is 28.8 corresponding to (040) of  $\text{SiO}_2$  phase (JCPDS 14-0654).

Magnetron sputtering deposited silver atoms on the surface of the structure and formed relatively uniform nanoparticles. As time goes on, the nanoparticles are connected or even merged to form larger nanoparticles. In SEM images, the results showed that the part of the spherical top increased, and the nanoparticles on the spherical top also increased. The general cause of fluorescence signal enhancement on metal nanostructures is electromagnetic field induced LSPR enhancement [24]. The active plasma sites are also referred to as "hot spots", which in this work could be divided into two types [25]. The first "hot spots" is the area closest to each other between the adjacent columns, which is because the nanogap decreases with the sputtering time increased. It can be seen from the observation of the FE-SEM image that as the sputtering time increases, the size of the nano-pillars increases continuously, and the column changes from a cylinder to a prism to occupy a gap space, so that the nanogap becomes very small. Some nanopillars are even connected together directly and the "hot spots" disappears. The second "hot spots" is the area between nanoparticles that sit next to each other on the same column. The electric field analysis can be seen in the numerical simulation section below.

### 3.2. Optical Properties

R6G was selected as the fluorophore probe because which is considered as a kind of very common fluorescence dye in the enhanced fluorescence research field and be used as laser dye. As shown in Figure 3., the absorption peak of R6G on Ag-C.W.-25 substrate was at 525 nm, and its effective absorption range can be 470-550 nm. Compared with neat cicada wing, the absorbance of substrates deposited silver significantly increased. After the deposition of silver, the maximum absorption wavelength appeared at 390 nm. With the increase of sputtering time to 25 min, the overall absorption increased and the peak slightly shifted to 386 nm. After sputtering  $\text{SiO}_2$ , the absorption was increased, and with the sputtering time prolonged, the absorption was slightly increased. The substrate showed a broad absorption, which was considered to contribute to the broad size distribution of the nanostructures that can cause SPR at different wavelength [26].

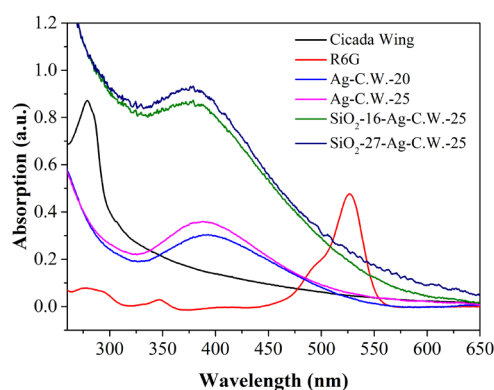


**Figure 3.** Absorption spectra of cicada wing (black), R6G aqueous solution (red), Ag-C.W.-20 substrate (blue), Ag-C.W.-25 substrate (purple) and  $\text{SiO}_2$ -16-Ag-C.W.-25 substrate (olive),  $\text{SiO}_2$ -27-Ag-C.W.-25 substrate (navy).

### 3.3. SEF Characteristics

#### 3.3.1. Substrate with different sputtering time of Ag

The fluorescence spectra of R6G aqueous solution on the substrates were shown in Figure. 4(a). Curves represented fluorescence intensities of Ag-C.W. substrates with 20 min, 22.5 min, 25 min, 30 min and 40 min sputtering time, respectively. Navy curve was for glass substrate without deposition

which was used as a reference. We can see that the fluorescence intensity signals of both dyes were obviously enhanced by the Ag-C.W. nanostructure substrates. The enhancement factors ( $E_f$ ) were calculated as follows:

$$E_f = \frac{I_{SEF} - I_{background}}{I_{reference} - I_{background}}, \quad (1)$$

where  $I_{SEF}$  is the fluorescence intensity of dye molecule on the substrates of Ag-C.W. nanostructures,  $I_{reference}$  is the fluorescence intensity of same volume of solution on the blank quartz substrate,  $I_{background}$  is the background of noise signal spectra intensity, respectively.  $E_f$  of 20 min, 22.5 min, 25 min, 30 min and 40 min substrates were 1.34, 1.53, 1.61, 1.50, 1.48, and were also shown in Figure. 4(b). From 20 min to 25 min, SEF effect becomes stronger with the increase of sputtering time on substrates. A monotonic decrease in fluorescence enhancement appeared as the sputtering time increased to 40 min. The result indicated that 25 min is the percolation threshold in this experiment.

According to the study of Geddes's group [27,28], the SEF phenomenon was based on the enhanced electromagnetic fields generated by the LSPR effects of metallic nanostructures. It only occurred in the nanospace less than 10 nm from the metallic surface. As schematic diagram, Figure 4.(c), shown that a little part of dye molecules which located in the nanogaps and on the top of the spherical top have the possibility of coupling with LSPR. According to Similar sandwich structure in the study of Zhang's group [29] and our previous work [30], correction calculation is necessary.

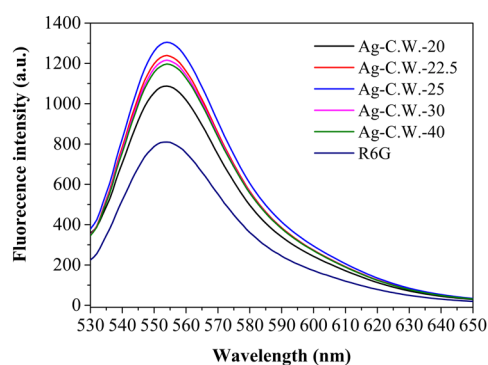
The average height of the unmodified nanopillars was measured as 390 nm, the thickness of Ag thickens after different modifications. So that the thickness of effective layer,  $h$ , could be considered as 500 nm. The height of the oblate column formed by solution droplet was regarded as the depth of the groove in quartz slide, 0.4 mm. We assumed that the intensity of non-enhanced part was  $Y$  per nanometer, while the enhanced part was  $X$  per nanometer. The total intensity equals to the not enhanced part plus the enhanced part, noted as

$$h \times X + (4 \times 10^5 - h) \times Y = 4 \times 10^5 \times E_f \times Y, \quad (2)$$

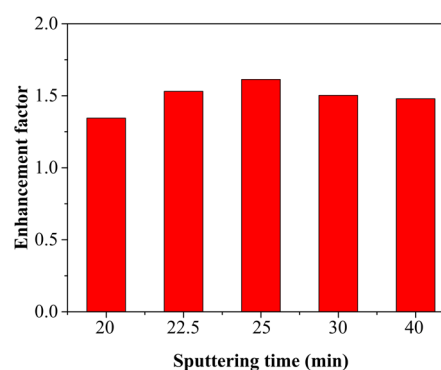
And the corrected enhancement factor

$$E_f' = X/Y, \quad (3)$$

The corrected enhance factor were also calculated and shown in Figure. 4 (d). The  $E_f'$  of 20 min, 22.5 min, 25 min, 30 min and 40 min substrates were 276.7, 425.8, 491.6, 103.3, 387.8, which reflects the real enhancement.



(a)



(b)

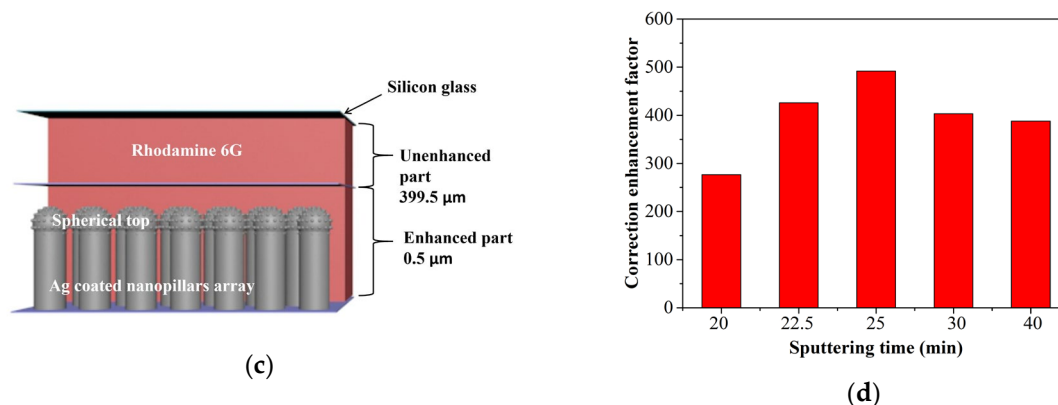


**Figure 4.** (a) The fluorescence spectra of different substrates for R6G: Ag-C.W.-20 substrate (black), Ag-C.W.-22.5 substrate (red), Ag-C.W.-25 substrate (blue), Ag-C.W.-30 substrate (magenta), Ag-C.W.-40 substrate (olive) and R6G solution on quartz substrate for reference (navy); (b) Enhancement factors of Ag-C.W.-x substrate with sputtering time from 20 to 40 mins; (c) The sandwich structure used in the surface enhanced fluorescence experiments; (d) Correction enhancement factors of Ag-C.W.-x substrate with sputtering time from 20 to 40 mins;

### 3.3.2. Substrate with different sputtering time of SiO<sub>2</sub>

The Ag-C.W.-22.5, Ag-C.W.-25, Ag-C.W.-30 was selected for further magnetron sputtering SiO<sub>2</sub> due to their good SEF effect. The fluorescence spectra of R6G aqueous solution on the SiO<sub>2</sub> coated substrates were shown in Figure 5.(a). The SEF effect of Ag-C.W.-22.5, Ag-C.W.-25 and Ag-C.W.-30 substrates after sputtering SiO<sub>2</sub> for 16s all enhanced. This proved that the separation layer does prevent fluorescence quenching. The next step is to explore the influence of different film thickness of SiO<sub>2</sub> controlled by sputtering time on Ag-C.W.-22.5, Ag-C.W.-30 substrate. The fluorescence spectra of different SiO<sub>2</sub> sputtering time (10 s, 16 s, 27 s) were measured, and their  $E_f$ s and  $E_f'$ s were calculated and shown in Figure 5.(b) and (c), respectively. The SEF effect of the three substrates increased first and then decreased as sputtering time increased. As shown in Table 2. after sputtering SiO<sub>2</sub> for 16 s, the  $E_f$  and  $E_f'$  of the substrates increased significantly compared with that without sputtering SiO<sub>2</sub> respectively.

**Table 2.** The enhancement factor of substrates before and after sputtering SiO<sub>2</sub> for 16 s.

Substrate name	$E_f$ after sputtering SiO <sub>2</sub>	$E_f'$ after sputtering SiO <sub>2</sub>	$E_f'$ before sputtering SiO <sub>2</sub>
Ag-C.W.-22.5	1.73	586.2	425.8
Ag-C.W.-25	1.81	649.4	491.6
Ag-C.W.-30	1.99	797.6	103.3

Interestingly, the one that got the best enhancement was not one, which was the best in bare metal substrates, but Ag-C.W.-30, which was slightly worse than Ag-C.W.-25. This is mainly because SiO<sub>2</sub> of appropriate thickness cancels quenching, so that the high electromagnetic field and high LSPR property caused by the original structure regain the dominant role [31]. After sputtering SiO<sub>2</sub> for 27 s, excessive SiO<sub>2</sub> occupied the remaining gap space, the probe molecules could not occupy the hot spot, and the fluorescence enhancement effect was reduced to that before coating. In Appendix A, FDTD was used to simulate the minimum repeating units of the corresponding structures of the above three substrates and the electric field distribution was obtained and two types hot spot distribution was confirmed. In the simulated electric field, the intensity of Ag-C.W.-30 is stronger than that of Ag-C.W.-25, but the actual SEF is weaker than that of 25 min. The experimental results show that the isolation layer of SiO<sub>2</sub> does play a role in preventing quenching.

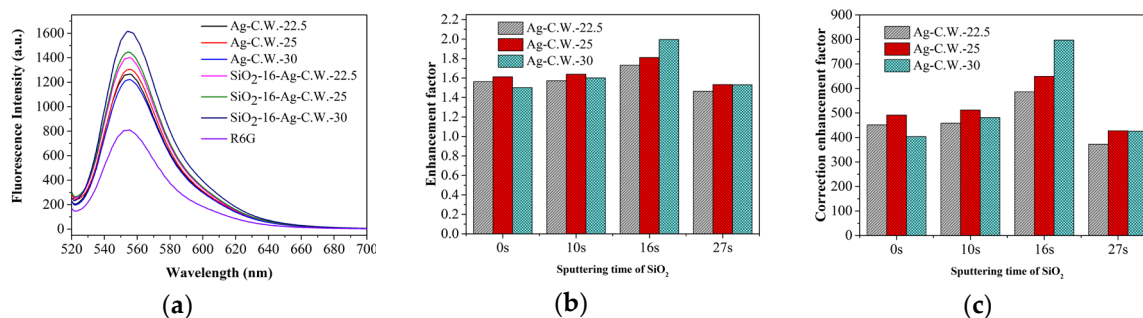


**Figure 5.** (a) The fluorescence spectra of different substrates for R6G: Ag-C.W.-22.5 substrate (black), Ag-C.W.-25 substrate (red), Ag-C.W.-30 substrate (blue), SiO<sub>2</sub>-16-Ag-C.W.-22.5 substrate (magenta), SiO<sub>2</sub>-16-Ag-C.W.-25 substrate (olive), SiO<sub>2</sub>-16-Ag-C.W.-30 (navy) and R6G solution on quartz substrate for reference (violet); (b) and (c) are the enhancement factors and correction enhancement factors of Ag-C.W.-22.5, Ag-C.W.-25, Ag-C.W.-30 substrate with sputtering time of SiO<sub>2</sub> from 0 to 27 seconds, respectively.

### 3.3.3. The sensitivity of the SEF substrate

Figure 6.(a) shows the SEF spectra of R6G with the concentration from  $10^{-2}$  to  $10^{-7}$  mol/L using the SiO<sub>2</sub>-16-Ag-C.W.-30 substrate, which indicated that the LOD was about  $1 \times 10^{-7}$  mol/L. The plot of fluorescence intensities for R6G also showed a well linear correlation with R6G concentration ranging from  $10^{-2}$  mol/L to  $10^{-7}$  mol/L, as shown in Figure 6.(b). The linear equation was  $y = 11404.45 + 1598.41x$  ( $x$  was the logarithm of R6G concentration;  $y$  was the fluorescence intensity), the correlation coefficient  $R^2$  was 0.978. The data proved that substrate had good sensitivity for detecting R6G fluorescence.

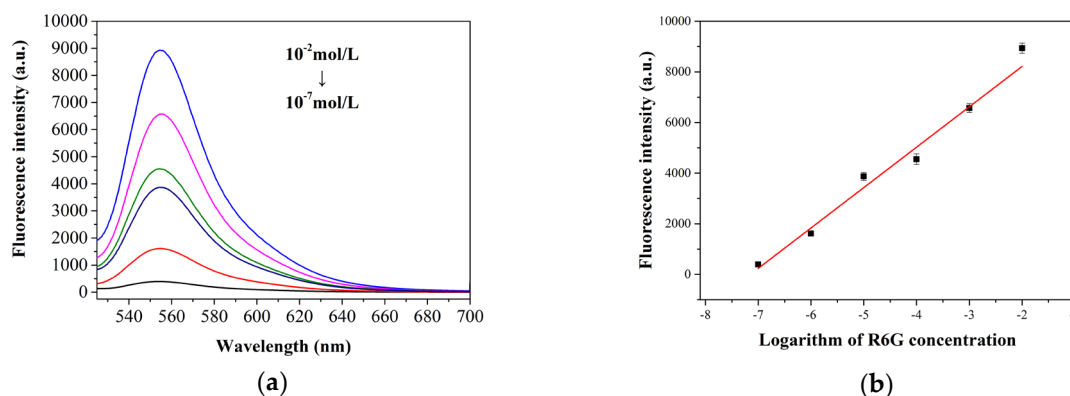


**Figure 6.** (a) Fluorescence spectra of R6G at different concentrations (from  $10^{-2}$  to  $10^{-7}$  mol/L). (b) Linear correlation of fluorescence intensities at 555 nm.

### 3.3.4. The stability of the SEF substrate

SEF became more extensive in application for detection in recent years, and the stability of SEF substrates is also increasingly important. The high-performance in stability lowers the usage amount in novel metal materials. It has commercial profit to lower the cost, and reduced environmental pollution. To test the stability of Ag-C.W.-25 and SiO<sub>2</sub>-16-Ag-C.W.-30 substrates, fluorescence spectra of R6G ( $10^{-6}$  mol/L) were collected after 0 week, 1 week, 2 weeks, 4 weeks, and 6 weeks of natural placement under the same conditions. Their fluorescence intensities at 555 nm were shown in Figure 7. The fluorescence intensity reduced as the placement time increased. For Ag-C.W.-25 substrates, the fluorescence intensity decreased by 4.5%, 9.1%, 14.3%, and 19.6% after 1 week, 2

weeks, 4 weeks and 6 weeks, respectively, mainly because the substrate was slightly oxidized as time pass away. For Ag-C.W.-25 substrates, the fluorescence intensity decreased by 0.4%, 0.8%, 1.5%, and 2% after 1 week, 2 weeks, 4 weeks and 6 weeks, respectively. The existence of SiO<sub>2</sub> isolation layer effectively block the oxidation process.

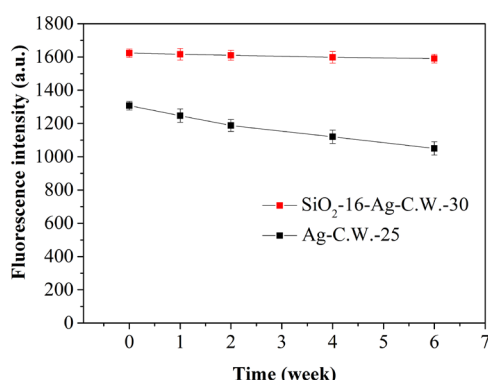


**Figure 7.** The fluorescence intensity of Ag-C.W.-25 and SiO<sub>2</sub>-16-Ag-C.W.-30 substrates of placement time for 1 week, 2 weeks, 4 weeks and 6 weeks.

### 3.3.5. The reproducibility of the SEF substrate

Reproducibility is an important index to ensure the validity of experimental data. As illustrated in Figure 8.(a) and (b), to test the reproducibility of SEF substrates, fluorescence spectra of R6G (10<sup>-6</sup> mol/L) were collected from twenty different locations on Ag-C.W.-25 and SiO<sub>2</sub>-16-Ag-C.W.-30 substrates, respectively. The column graphs of Figure 8.(c) and (d) show that the relative RSD estimated by the fluorescence intensities of 555 nm were 4.24% and 4.37%, respectively. The data indicated that whether there is SiO<sub>2</sub> separation layer or not, Ag-C.W. substrate had favorable reproducibility for detecting R6G fluorescence.

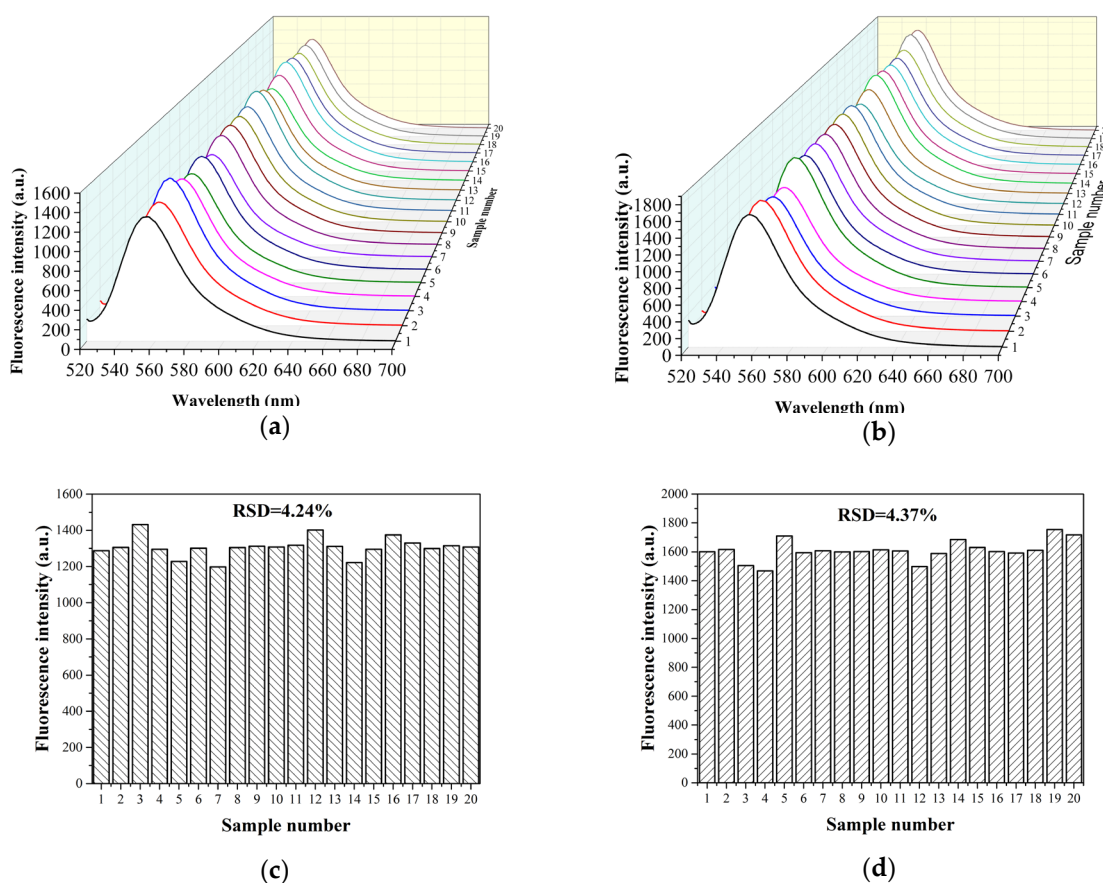


**Figure 8.** (a) Fluorescence spectra of  $10^{-6}$ mol/L R6G collected from twenty randomly selected samples. (b) Fluorescence spectra of  $10^{-6}$ mol/L R6G on SiO<sub>2</sub>-16-Ag-C.W.-30 collected from twenty randomly selected samples. (c) the RSD of the fluorescence intensity of R6G on Ag-C.W.-25 at 555 nm. (d) the RSD of the fluorescence intensity of R6G on SiO<sub>2</sub>-16-Ag-C.W.-30 at 555 nm.

#### 4. Conclusion

In this work, we have studied the Ag-cicada wing and SiO<sub>2</sub>-Ag-cicada wing substrates fabricated by magnetron sputtering with the purpose to prove the SEF's enhancement capabilities, in which R6G was selected as fluorescent probe. The Ag-cicada wing substrate's structure consisting of nano-pillars array, and nano-particles with strong LSPR was produced deposited Ag on the cicada wing skeleton in nanoscale, give new possibility in SEF. The fluorescence intensity increased first with the increase of sputtering time, and reached a peak at 25 min. After 25 minutes, the nano-gaps of the structure was gradually filled by sputtering, which caused SEF to decline slowly. The intensity of the R6G fluorescence on the Ag-C.W.-25 substrate was enhanced with correction enhancement factor of 491.6, which is attributed to the LSPR and "hot spots" from the its structure. SiO<sub>2</sub> was introduced as the separation layer on Ag-cicada substrate and the SiO<sub>2</sub>-16-Ag-C.W.-30 one obtain higher enhancement with correction fluorescence enhancement factor of 797.6. The best enhancement was achieved on the 30 mins one rather than the 25 mins one in the SiO<sub>2</sub> coated Ag-C.W. substrate, proving that deposited SiO<sub>2</sub> successfully prevented fluorescence quenching and revealed enhancement property of the substrate itself. FDTD was used to simulate the electromagnetic field enhancement distribution of the substrate with different sputtering time, and the "hot spots" distribution and cause were analyzed. Fluorescence signals of substrates with spacer layer or not exhibited good reproducibility with the relative standard deviation value of 4.24% and 4.37%, respectively. Moreover, the substrate exhibited sensitivity with the limits of detection (LOD) as low as  $1 \times 10^{-7}$  mol/L and high stability with 2% decrease in fluorescence intensity after oxidation for 6 weeks under natural conditions. We propose that SEF substrate with high reproducibility and stability has broad application prospects in biomedical investigations.

**Funding :** This research was funded by Scientific and Technological Research Key Projects of Colleges and Universities in Hebei province (ZD2019069).

**Conflicts of Interest:** The authors declare no conflict of interest.

#### Appendix A

##### 3D finite-difference time-domain simulation

The Ag-coated nanopillars has an effective LSPR under the excitation of 500 nm, which makes the local field strength stronger in the gap. The distance between nanoparticles has an important effect on near-field enhancement. Therefore, the electromagnetic intensity distribution is simulated using a three-dimensional finite difference time domain method (3D-FDTD) [30,32]. In order to reproduce the base morphology of 22.5 min, 25 min and 30 min, two parallel columns of nanopillars were set with a spacing of 197 nm (Measured). Two parallel nanocolumns can be considered as the smallest repeating unit of the substrate. The model uses Ag as the surface and the surface is covered with Ag nanoparticles with a diameter of 10 nm. The average height of the column was set to 200 nm, and the diameter of the dome was set to 165 nm, 185 nm, and 192 nm, respectively, based on FE-SEM images. As shown in Figure A.(a)-(c), the closest gaps between the two nanostructures at the edge of the dome are 32 nm, 12 nm, and 5 nm, respectively. In addition, a continuous square wave having a wavelength of 500 nm was selected as the incident light. We believe that Ag is in line with the Debye-Drude model.

Figure A. (d)-(f) are planes in which the center of the top of the column is parallel to the x-y plane, and Figure A. (g)-(i) are diagrams showing the electric field intensity distribution of the x-z. As shown in Figure A. (d) and (g), two kinds of hotspots were involved in the field enhancement, one

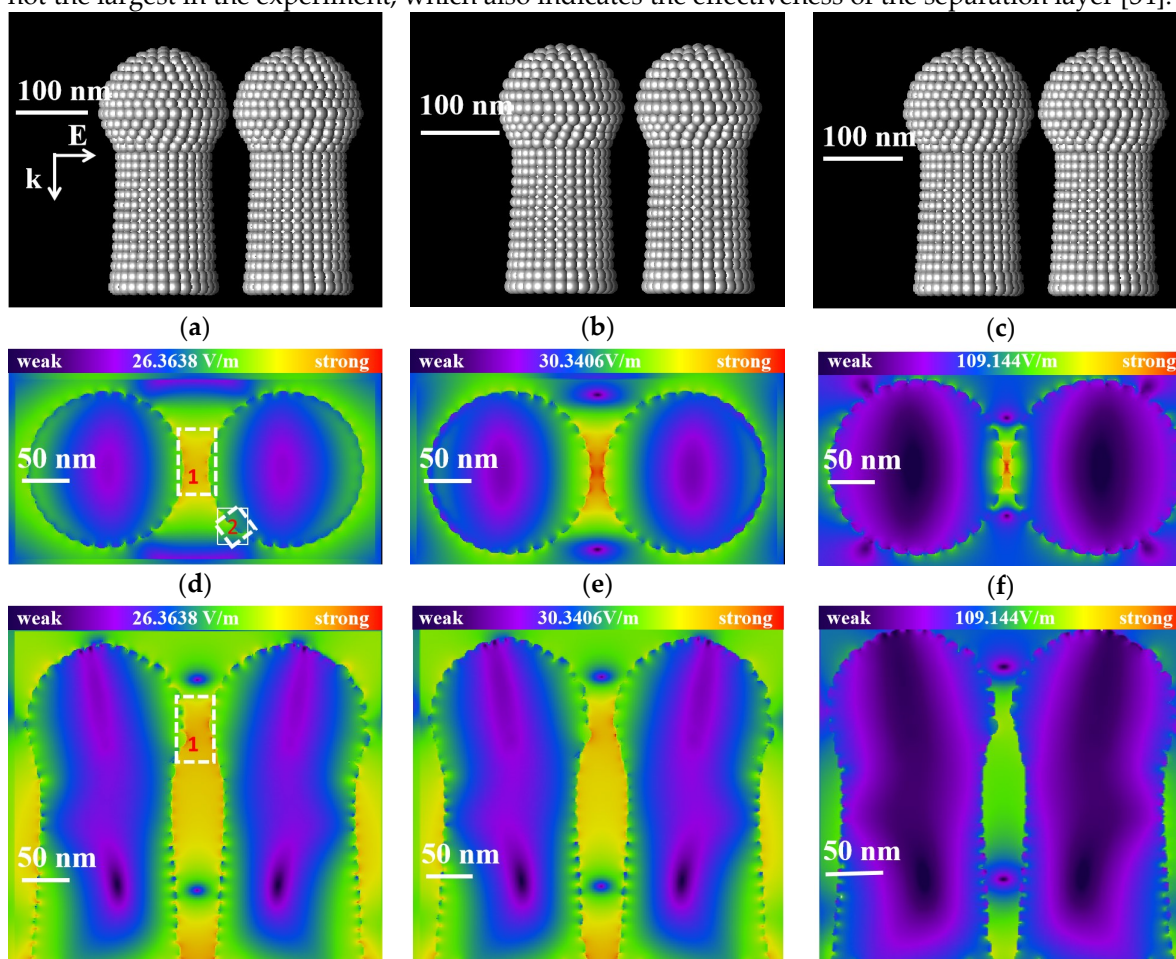
is at the closest place of adjacent columns, and the other is between the nanoparticles on surface. The strong electromagnetic field strength is distributed in the nano-gap between the Ag nanoparticles on the surface of the sphere. The total electric field strength reference value is given separately. It is clear that the electromagnetic field enhancement of the Ag-C.W.-30 substrate is stronger than other substrates. This enhanced local electromagnetic field can improve excitation efficiency and emission efficiency. However, this enhanced local electromagnetic field can increase the excitation and emission efficiency of both metal surfaces as well as the non-radiative decay rate. According to J.R. Lakowicz 's study [24],

$$C_{ext} = C_{sca} + C_{abs} \quad (4)$$

$$C_{sca} = \frac{8\pi}{3} k^4 a^6 |\alpha|^2 \quad (5)$$

$$C_{abs} = 4\pi k a^3 \text{Im}(\alpha) \quad (6)$$

Where  $C_{ext}$ ,  $C_{sca}$ ,  $C_{abs}$  are the cross section of extinction, scattering and absorption, respectively.  $k$  is defined as incident wavevector,  $a$  is the radius Ag nanoparticles and  $\alpha$  is polarizability of Ag nanoparticles. The scattering cross section which leads to fluorescence enhancement is proportional to the sixth power of the radius of the silver nanoparticles, and the absorption cross section which leads to quenching is proportional to the third power of the radius of the silver nanoparticles [33]. As sputtering time goes by, the Ag nanoparticles grow bigger, and the radius and scattering cross section increase. But the closer reporters located to the metal surface, the lower their quantum yield. This explains that Ag-C.W.-30 has the largest electromagnetic field enhancement in simulation, but not the largest in the experiment, which also indicates the effectiveness of the separation layer [34].



(g) (h) (i)

**Figure A.** (a)-(c) The model of the nanocolumns which covered with Ag to restore the morphology of Ag-C.W.-22.5, Ag-C.W.-20 and Ag-C.W.-30, respectively; The spatial distribution of the electromagnetic field intensity ; (d)-(f) the plane with the center of the sphere on the top of column paralleled to the x-y planes, for Ag-C.W.-22.5, Ag-C.W.-25 and Ag-C.W.-30, respectively; (g)-(i) the plane passing through the axis of two cylinders, for Ag-C.W.-22.5, Ag-C.W.-25 and Ag-C.W.-30, respectively.

## References

1. Liu Y, Dong P, Jiang Q, et al. Assembly-enhanced fluorescence from metal nanoclusters and quantum dots for highly sensitive biosensing. *Sensors and Actuators B: Chemical*, **2019**, 279, 334-341.
2. Chen T, Pei X, Yue Y, et al. An enhanced fluorescence sensor for specific detection Cys over Hcy/GSH and its bioimaging in living cells. *Spectrochimica Acta Part A: Molecular and Biomolecular Spectroscopy*, **2019**, 209,223-227.
3. Knoblauch R, Geddes C D. Silvered conical-bottom 96-well plates: enhanced low volume detection and the metal-enhanced fluorescence volume/ratio effect. *Nanoscale*, **2019**, 11, 4337-4344.
4. Ning P, Wu Z, Li X, et al. Development of functionalized gold nanoparticles as nanoflare probes for rapid detection of classical swine fever virus. *Colloids and Surfaces B: Biointerfaces*, **2018**, 171, 110-114.
5. Doré K, Leclerc M, Boudreau D. Investigation of a fluorescence signal amplification mechanism used for the direct molecular detection of nucleic acids. *Journal of fluorescence*, **2006**, 16, 259-265.
6. Geddes C D, Lakowicz J R. Metal-enhanced fluorescence. *Journal of fluorescence*, **2002**, 12, 121-129.
7. Shalon D, Smith S J, Brown P O. A DNA microarray system for analyzing complex DNA samples using two-color fluorescent probe hybridization. *Genome research*, **1996**, 6, 639-645.
8. Johansson P, Xu H, Käll M. Surface-enhanced Raman scattering and fluorescence near metal nanoparticles. *Physical Review B*, **2005**, 72, 035427.
9. Ding S Y, You E M, Tian Z Q, et al. Electromagnetic theories of surface-enhanced Raman spectroscopy. *Chemical Society Reviews*, **2017**, 46, 4042-4076.
10. Xu H, Wang X H, Persson M P, et al. Unified treatment of fluorescence and Raman scattering processes near metal surfaces. *Physical review letters*, **2004**, 93, 243002.
11. Anger P, Bharadwaj P, Novotny L. Enhancement and quenching of single-molecule fluorescence. *Physical review letters*, **2006**, 96, 113002.
12. Zhang Z, Yang P, Xu H, et al. Surface enhanced fluorescence and Raman scattering by gold nanoparticle dimers and trimers. *Journal of Applied Physics*, **2013**, 113, 033102.
13. Aslan K, Lakowicz J R, Szmajcinski H, et al. Metal-enhanced fluorescence solution-based sensing platform. *Journal of fluorescence*, **2004**, 14, 677-679.
14. Brolo A G, Kwok S C, Moffitt M G, et al. Enhanced fluorescence from arrays of nanoholes in a gold film. *Journal of the American Chemical Society*, **2005**, 127, 14936-14941.
15. Dragan A I, Bishop E S, Casas-Finet J R, et al. Distance dependence of metal-enhanced fluorescence. *Plasmonics*, **2012**, 7, 739-744.
16. Ray K, Badugu R, Lakowicz J R. Polyelectrolyte layer-by-layer assembly to control the distance between fluorophores and plasmonic nanostructures. *Chemistry of Materials*, **2007**, 19, 5902-5909.
17. Li J F, Zhang Y J, Ding S Y, et al. Core-shell nanoparticle-enhanced Raman spectroscopy. *Chemical reviews*, **2017**, 117, 5002-5069.
18. Xu J, Zhang Y J, Yin H, et al. Shell-Isolated Nanoparticle-Enhanced Raman and Fluorescence Spectroscopies: Synthesis and Applications. *Advanced Optical Materials*, **2018**, 6.
19. Jeong Y, Kook Y M, Lee K, et al. Metal enhanced fluorescence (MEF) for biosensors: General approaches and a review of recent developments. *Biosensors and Bioelectronics*, **2018**, 111,102-116.
20. Deng Y L, Xu D D, Pang D W, et al. Target-triggered signal turn-on detection of prostate specific antigen based on metal-enhanced fluorescence of Ag@SiO<sub>2</sub>@SiO<sub>2</sub>-RuBpy composite nanoparticles. *Nanotechnology*, **2017**, 28, 065501.
21. Yan Y, Meng L, Zhang W, et al. High-throughput single-particle analysis of metal-enhanced fluorescence in free solution using Ag@ SiO<sub>2</sub> core-shell nanoparticles. *ACS sensors*, **2017**, 2, 1369-1376.

22. Wang Y, Wang M, Sun X, et al. Grating-like SERS substrate with tunable gaps based on nanorough Ag nanoislands/moth wing scale arrays for quantitative detection of cypermethrin. *Optics express*, **2018**, *26*, 22168-22181.
23. Yan X, Wang M, Sun X, et al. Sandwich-like Ag@Cu@CW SERS substrate with tunable nanogaps and component based on the Plasmonic nanonodule structures for sensitive detection crystal violet and 4-aminothiophenol. *Applied Surface Science*, **2019**, *479*, 879-886.
24. Lakowicz J R. Radiative decay engineering 5: metal-enhanced fluorescence and plasmon emission. *Analytical biochemistry*, **2005**, *337*, 171-194.
25. Kleinman, S.L.; Frontiera, R.R.; Henry, A.-I.; Dieringer, J.A.; Van Duyne, R.P. Creating, characterizing, and controlling chemistry with SERS hot spots. *Phys. Chem. Chem. Phys.* **2013**, *15*, 21–36.
26. Bosman, M.; Anstis, G.R.; Keast, V.J.; Clarke, J.D.; Cortie, M.B. Light Splitting in Nanoporous Gold and Silver. *ACS Nano* **2012**, *6*, 319–326.
27. Zhang Y, Dragan A, Geddes C D. Metal-enhanced fluorescence from tin nanostructured surfaces. *Journal of Applied physics*, **2010**, *107*, 024302.
28. Aslan K, Malyn S N, Zhang Y, et al. Conversion of just-continuous metallic films to large particulate substrates for metal-enhanced fluorescence. *Journal of applied physics*, **2008**, *103*, 084307.
29. Zhang Y, Yang C, Xiang X, et al. Highly effective surface-enhanced fluorescence substrates with roughened 3D flowerlike silver nanostructures fabricated in liquid crystalline phase. *Applied Surface Science*, **2017**, *401*, 297-305.
30. Shang Z, Wang M, Pan S, et al. Ag@DWs nanopillars as a nanoprobe for detection of R6G via surface-enhanced fluorescent. *Optics Communications*, **2019**, *451*, 345-352.
31. Reineck P, Gómez D, Ng S H, et al. Distance and wavelength dependent quenching of molecular fluorescence by Au@ SiO<sub>2</sub> core-shell nanoparticles. *ACS nano*, **2013**, *7*, 6636-6648.
32. Surface plasmon enhanced, coupled and controlled fluorescence. John Wiley & Sons, **2017**.
33. J. Lukomska, J. Malicka, I. Gryczynski, Z. Leonenko, J.R. Lakowicz, Fluorescence enhancement of fluorophores tethered to different sized silver colloids deposited on glass substrate, *Biopolymers*, **2005**, *77*, 31–37.
34. Aslan K, Leonenko Z, Lakowicz J R, et al. Annealed silver-island films for applications in metal-enhanced fluorescence: interpretation in terms of radiating plasmons. *Journal of fluorescence*, **2005**, *15*, 643.